Int. J. Heat Mass Transfer. Vol. 27, No. 2, pp. 233–242, 1984
Printed in Great Britain

0017–9310/84 $3.00 + 0.00

HEAT TRANSFER ADJACENT TO THE ATTACHED END OF A CYLINDER IN CROSSFLOW

E. M. SPARROW, T. J. STAHL and P. TRAUB
Department of Mechanical Engineering, University of Minnesota, Minneapolis, MN 55455, U.S.A.

(*Received* 11 *April* 1983 *and in revised form* 26 *May* 1983)

Abstract—Wind tunnel experiments were performed to determine heat transfer coefficients in the region of wall–cylinder interaction for a wall-attached cylinder in crossflow. Quasi-local transfer coefficients were measured with a small (one-quarter diameter long) disk-like sensing element positioned at various axial stations along the cylinder. The experiments spanned the Reynolds number range from 3500 to 23 000 and were supplemented by velocity profile measurements and flow visualization. It was found that the wall–cylinder interactions were confined to a length of the cylinder extending about one diameter from the wall. In the interaction region, the quasi-local coefficients were lower than those in the wall-unaffected region. The decreases were accentuated with decreasing distance from the wall, but this trend was reversed in the immediate neighborhood of the wall due to the presence of a compact, vigorous vortex. The largest decrease was in the 15% range, while the average decrease for the entire wall-affected region was about 9%.

NOMENCLATURE

d	cylinder diameter
$\mathscr{D}$	diffusion coefficient
K	mass transfer coefficient, $\dot{m}/(\rho_{nw}-\rho_{n\infty})$
$\dot{m}$	average mass flux at sensor surface
Re	Reynolds number, $u_\infty d/\nu$
Sh	Sherwood number, $Kd/\mathscr{D}$
Sc	Schmidt number
u	velocity at distance y from wall
u_∞	freestream velocity
y	distance from wall.

Greek symbols

ν	kinematic viscosity
ρ_{nw}	naphthalene vapor density at subliming surface
$\rho_{n\infty}$	naphthalene vapor density in freestream.

INTRODUCTION

THE CYLINDER in crossflow is one of the most frequently encountered heat transfer configurations and, as a consequence, it has been the subject of extreme experimental study as witnessed in refs. [1, 2]. In general, either one or both ends of such cylinders are attached perpendicular to a wall. At the wall–cylinder interface and extending along the cylinder for a yet-undetermined distance, the fluid flow passing over the cylinder interacts with the wall-adjacent boundary layer. The heat transfer ramifications of these interactions have long been a matter of speculation, especially in connection with applications such as pin fins and tube banks. In view of the importance of the problem, it is remarkable that cylinder heat transfer coefficients for the region adjacent to the wall–cylinder attachment are unavailable in the published literature.

A logical starting point for the study of wall–cylinder interactions is the case of the single cylinder in crossflow. Furthermore, to ensure that the measured end-adjacent heat transfer coefficients truly reflect the wall–cylinder interactions, the cylinder should be long enough so that hydrodynamic and thermal happenings at the other end do not influence the region of interest. Such end-to-end interactions, which are expected to be important only for relatively short cylinders, merit separate study. The problem of wall–cylinder interactions in tube banks also requires separate study, but conjectures about the importance of these effects may be guided by results from the single cylinder case. This matter will be revisited at the end of the paper.

The present experiments were performed with a single cylinder in crossflow, one of whose ends was attached perpendicular to the wall of a wind tunnel while the other end was free. The length of the cylinder was such that there were no interactions between the respective ends. The work encompassed two separate but interrelated foci. In the main body of experiments, quasi-local heat transfer coefficients were measured at the cylinder surface for a sequence of axial stations starting at the wall–cylinder interface and progressing along the cylinder in the direction away from the wall. Baseline measurements were also made at a location far from both ends of the cylinder. These experiments spanned the Reynolds number range from about 3500 to 23 000.

The second focus of the research was concerned with the fluid flow characteristics. It consisted of two parts. In one, velocity profiles were measured at the site of the cylinder (with the cylinder removed) in order to establish the thickness of the velocity boundary layer in the flow approaching the cylinder. In the second, flow visualizations were made using the oil–lampblack technique. These visualizations provided insights into the patterns of fluid flow both on the cylinder and on the wall adjacent to the attachment of the cylinder.

The only related results found by the authors were contained in an unpublished report by Karni [3]. That investigation was limited to a single Reynolds number of 19 000. For completeness, mention may be made of published information [4] on heat transfer at and adjacent to the free end of a single cylinder in crossflow.

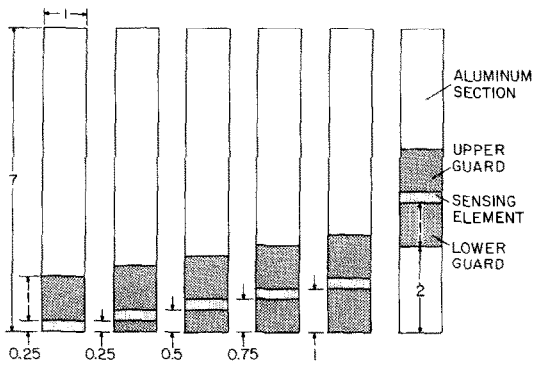

FIG. 1. Crossflow cylinders used during the research.

EXPERIMENTS

To obtain quasi-local heat transfer coefficients possessing both high accuracy and a high degree of resolution, it is advantageous to employ the naphthalene sublimation technique instead of direct heat transfer measurements. The dimensionless mass transfer results (Sherwood numbers) obtained from the naphthalene technique can be transformed to Nusselt numbers for heat transfer via the analogy between the two processes. In addition to greater measurement precision, the special advantages of the naphthalene technique for the present problem are the virtual absence of extraneous losses (such as conduction in the corresponding heat transfer problem) and the easy attainment of a standard boundary condition (analogous to uniform wall temperature). The absence of conduction-like losses means that a local naphthalene-coated sensing element need be guarded only to ensure a proper convective environment. In the corresponding heat transfer problem, guard heaters must be employed (often with only partial success) both to minimize conduction and to establish the desired convective surroundings.

Experimental apparatus

A total of six cylinders were employed during the course of the experiments in order to obtain the sought-for resolution of the axial variation of the mass transfer coefficient. During any given data run, only one cylinder was employed. A schematic diagram showing an assemblage of all the test cylinders is shown in Fig. 1. When in place during a data run, the lower end of each cylinder was attached to the floor of a wind tunnel, while the upper end was free.

As seen in Fig. 1, each cylinder consisted of several parts. These included the local sensing element, the upper and lower guard sections which flanked the sensing element, and metallic (aluminum) sections which comprise the remainder of each cylinder. The sensing element and the guard sections presented naphthalene-coated surfaces to the airflow, while the metallic sections did not participate in the mass transfer process. The lengths of the metallic sections were chosen to give all the cylinders a uniform length equal to seven diameters.

Further inspection of Fig. 1 shows the positioning sequence of the sensing element. Starting from the LHS of Fig. 1, where the sensor is situated at the lower extremity of the cylinder, and proceeding to the right, the sensor is seen to be positioned at increasingly greater distances from the wall–cylinder interface. The axial length of the sensing element is equal to one-quarter of the cylinder diameter. Furthermore, its position from the wall–cylinder interface was incremented by one-quarter diameter intervals up to and including the fifth cylinder of the assemblage. The five leftmost cylinders, for which the overall range of the sensor extended to $1\frac{1}{4}$ diameters from the wall–cylinder interface, were employed to obtain mass transfer data for the wall-affected region.

For the rightmost cylinder, the sensor was positioned in the interval 3–$3\frac{1}{4}$ diameters from the wall–cylinder interface. Flow visualization studies, to be described later, had demonstrated that this site was remote from the effects of both the free end and the attached end of the cylinder. Consequently, the mass transfer results obtained with the rightmost cylinder were employed as baseline information both for comparison with the results for the wall-affected region and with heat transfer results from the literature.

It is relevant to discuss the function of the guard sections. To precisely model a uniform temperature cylinder by the heat–mass transfer analogy, the entire surface of the cylinder should be of naphthalene. However, in reality, convective mass (or heat) transfer interactions between axially separated stations occur only between closely spaced stations. Even in the wall-affected region for the present experiments, axial interactions extended over about a length of one diameter. Therefore, it was only necessary to flank the sensing element with naphthalene-coated sections (the guard sections) that were long enough to span the region of axial interactions. The guard sections shown in Fig. 1 were chosen on this basis, and supplementary runs with longer guards were made to verify their sufficiency. The motivation for not casting the entire cylinder in naphthalene was to reduce the time and complexity of preparing the apparatus for each data run.

Precise alignment of the sections is essential if a composite cylinder is to accurately model a continuous cylindrical surface. To ensure the quality and repeatability of the alignment, the sections which comprised any one cylinder were never interchanged with those of any other cylinder. The individual sections of each cylinder were custom fitted to each other to within rigid tolerances (< 0.00254 cm).

The nominal diameter of each respective cylinder was 2.54 cm, with no one cylinder deviating from the nominal by more than 0.3%.

Sensing elements and guard sections

A schematic cross sectional view of a sensing element

is shown in Fig. 2. As seen there, the element is, in essence, an annular disk whose outer periphery was recessed to provide a cavity which contains naphthalene implanted by a casting process. The naphthalene layer is bounded above and below by thin metallic rims whose exposed tips are approximately 0.01 cm thick. The rims served to prevent possible abrasion of the naphthalene which might have occurred in their absence due to contact with the guard sections. Further, the rims provided mechanical strength and a precisely machined surface for aligning the sections of the assembled cylinder.

It is also shown in Fig. 2 that the internal wall of the upper rim is canted upward away from the tip. This feature was provided to ensure that any bubbles present during the casting process would migrate away from the exposed surface of the naphthalene. The external surface of the upper rim was canted at a somewhat larger angle than the internal wall so as to produce a thickening of the rim in the direction away from its exposed tip. Also, the lower rim was angled so as to match the bevel of the upper surface of the guard section which it contacted.

The discrete steps in the upper and lower faces of the element mated with similar steps in the guard sections, thereby providing a tongue-in-groove type fit. The 0.635 cm diameter hole along the axis of the element was made to accommodate a center rod which served to hold the cylinder assembly together.

The upper guard section was very similar in design to the sensing element but was one diameter in length rather than one-quarter diameter in length. The lower guard section also was of similar design but, as shown in Fig. 1, was fabricated in various lengths ranging from one-quarter to one diameter. Also, in recognition of the fact that the lower guard rested on a flat surface (i.e. the floor of the wind tunnel), its base was not stepped as were the bases of the other sections. The base was, however, beveled so that it contacted the wind tunnel floor only along its outer rim, thereby aiding in the thermal isolation of the cylinder from the tunnel floor.

The various sections of the assembled cylinder were tied together by a center rod whose upper end was threaded into the aluminum section which comprised the upper portion of the cylinder. The lower end of the tie rod passed through the floor of the wind tunnel, where it was fixed in place by a retaining nut.

Attention will now be turned to the casting procedure used to implant the naphthalene in the sensing elements and the guards. An identical procedure was employed for all the elements and guards, so that it is only necessary to consider a representative piece, e.g. a sensing element. The first step in the procedure was to remove the naphthalene remaining from a prior data run by melting and evaporation. Then, a cylindrical brass sleeve was slipped over the sensor, such that the tips of the sensor rims just contacted the inner surface of the sleeve. The sleeve served as the outer boundary of the now-vacant mold cavity. Molten naphthalene was then poured into the cavity through a small hole in the upper face of the sensor, the pouring operation being facilitated by the use of a funnel which mated with the hole. The air displaced from the cavity escaped through a second, identical hole, also equipped with a funnel.

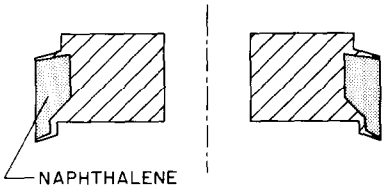

FIG. 2. Schematic cross sectional view of a sensing element.

Once the naphthalene had solidified, the sensor was separated from the sleeve by finger pressure applied from below. The separation was easily accomplished because the inner surface of the sleeve had been lapped to a mirror finish. The finish of the exposed surface of the naphthalene was of comparable quality.

The same sleeve was used in the casting of all the sections to ensure that all would have the same external diameter. When all the naphthalene-surface sections for a particular cylinder assembly had been cast, they were stacked together and a brass shrouding sleeve slid over the stack to prevent sublimation. For each set of sensors and guards, there was a specific shrouding sleeve whose length was precisely equal to the height of the stack. Impermeable tape was used for sealing at the top and bottom of the stack.

Instrumentation, experimental setup and procedure

Each sensor was equipped with a permanently installed chromel–constantan thermocouple (Teflon-coated, 0.025 cm wire). The thermocouple was embedded in the naphthalene, with its junction positioned about 0.02 cm from the surface exposed to the airflow. Each of the thermocouples was calibrated after installation in its respective sensor. In the experimental setup, the thermocouple lead wires were ducted through the center hole of the cylinder and brought out from the underside of the wind tunnel floor. This lead-out arrangement avoided any possible flow disturbances which might have resulted had the lead wires been drawn from the outside of the cylinder. The thermocouple e.m.f.'s were read with a 1 μV digital voltmeter.

The experiments were performed in a low-turbulence (0.3–0.4%) wind tunnel operated in the open-circuit mode. The tunnel test section was rectangular, 30.5 × 61 cm, vertical × horizontal. The cylinder was oriented vertically and positioned midway between the tunnel side walls. As already noted, it was attached to the floor of the tunnel, and there was a gap of 12.7 cm between its free end (i.e. upper end) and the upper wall of the tunnel.

The cylinder was situated 91 cm downstream of the inlet of the tunnel test section. To ensure the existence of a well-developed turbulent boundary layer, a trip wire (0.157 cm diameter) was installed at the leading edge of

the floor of the test section. At the lowest velocity of the experiments (cylinder Reynolds number of about 3500), the thickness of the boundary layer at the site of the cylinder was about 3.2 cm.

Data were collected over a range of wind tunnel freestream velocities u_∞ from 2.2 to 14.7 m s^{-1}, with a corresponding range of the cylinder Reynolds number from 3500 to 23 000. The freestream velocity was measured with a 0.076 cm diameter, circular impact tube situated slightly forward of and above the cylinder, with an adjacent wall tap used for the static pressure.

The same impact tube was employed to determine boundary layer velocity profiles adjacent to the floor of the wind tunnel at the vacant site of the test cylinder. For this purpose, the probe was introduced into the flow through a small hole in the floor of the tunnel (the same hole otherwise used for the center rod of the cylinder).

The difference between the impact and static pressures was sensed by an MKS Baratron capacitance-type, solid-state pressure meter capable of discriminating 10^{-3} Torr. The same instrument was employed to determine the tunnel static pressure (relative to ambient), while a precision barometer provided the ambient pressure.

Each data run was initiated with freshly cast naphthalene-surfaced components. Prior to its installation in the wind tunnel, the sensing element was weighed utilizing a Sartorius ultra-precision, electronic analytical balance with a smallest scale reading of 10^{-5} g. Then, the test cylinder was assembled, and a brass shrouding sleeve was slipped over the naphthalene-coated components and taped at the ends. The shroud and taping served to prevent sublimation, as was verified in auxiliary experiments. The cylinder was then placed in the wind tunnel, which had already been warmed up at the preselected freestream velocity.

The shrouded cylinder was allowed to attain thermal equilibrium with the airflow, as witnessed by the readings of the thermocouple embedded in the sensing element. Once equilibrium had been attained, the shroud was removed and the data run initiated. The duration of the run was chosen so as to limit the mean sublimation-related change in diameter to less than 0.0025 cm. To conclude the run, the shroud was slipped over the sensor and the guards. After the cylinder was removed from the wind tunnel and disassembled, the sensor was weighed (with the shroud removed). The amount of mass transfer was determined by differencing the weighings made before and after the run.

Flow visualization

The oil–lampblack technique was employed to enable visualization of the pattern of fluid flow adjacent to the lower portion of the cylinder and adjacent to the wind tunnel floor in the vicinity of the cylinder. The general procedure for using this technique is to brush a mixture of oil and lampblack powder on a surface and then to expose the surface to the airflow whose characteristics are to be studied. Under the action of the stresses exerted by the fluid, the mixture will move along the surface, producing a streak pattern indicative of the paths of the fluid particles which pass adjacent to the surface. However, in regions of low velocity (e.g. stagnation or reattachment zones), the stresses are small, so that the mixture remains virtually stationary, with the result that such regions show themselves as black streak-free zones on the surface.

The visualization runs were performed separately from the mass transfer data runs. For these runs, the surface was covered by white, plasticized contact paper to give the highest possible contrast for the black streak lines induced by the flow. Numerous trial mixtures were employed before one was found which provided high resolution of the flow pattern while resisting the tendency to sag when applied to the surface of the cylinder (which was vertical).

In order to obtain the most definitive possible patterns, the final visualization runs were made at the maximum velocity of the wind tunnel, which corresponds to a cylinder Reynolds number of about 32 000. Once the patterns were formed, the contact paper was removed from the surface and laid flat. The sharpest patterns were photographed and will be displayed shortly.

FLUID FLOW RESULTS

Flow visualization

The results of the flow visualization are presented via the photographs of Figs. 3 and 4 and by a diagram (Fig. 5) which sets forth a hypothesized view of the flow field.

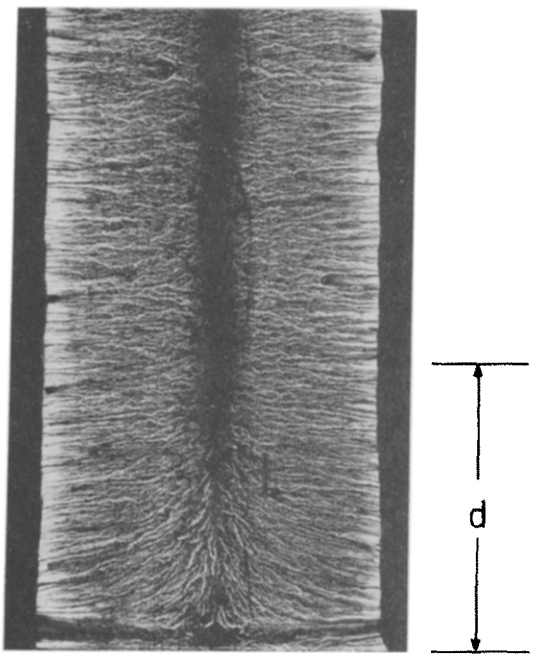

FIG. 3. Photograph of the flow pattern adjacent to the forward-facing portion of the cylinder.

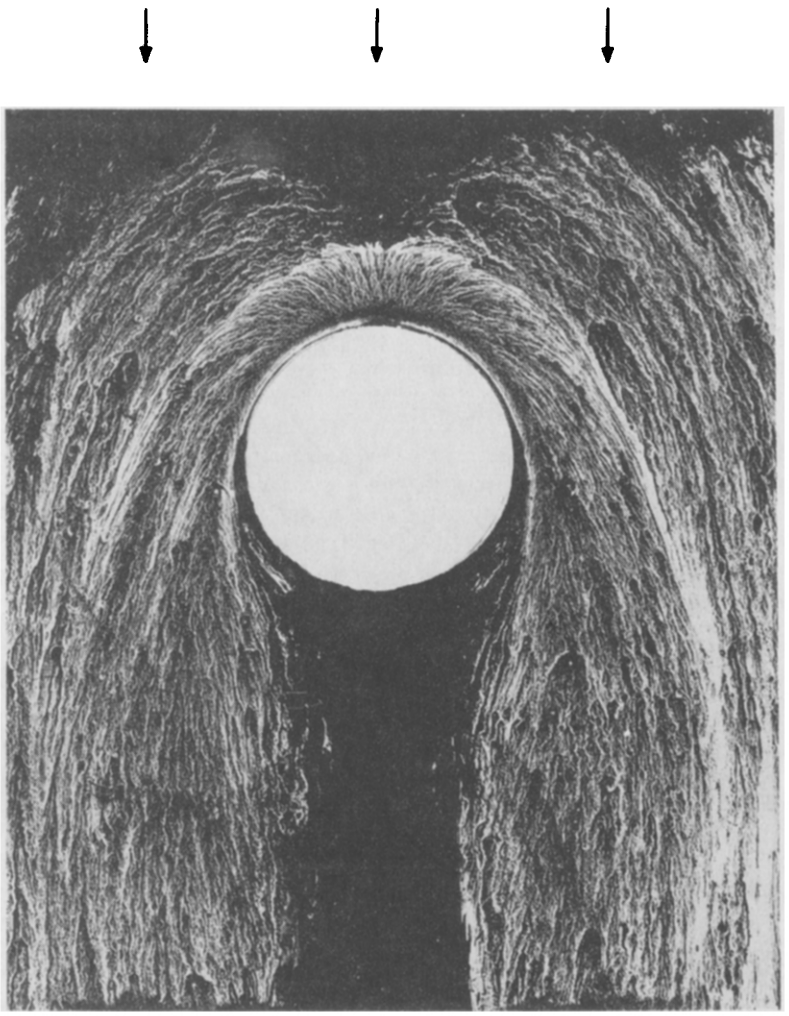

FIG. 4. Photograph of the flow pattern adjacent to the wind tunnel floor.

Figure 3 shows the flow pattern adjacent to the forward-facing portion of the cylindrical surface as viewed from a vantage point upstream of the cylinder. The upper edge of Fig. 3 corresponds to a position about 2.2 diameters above the base of the cylinder (i.e. above the floor of the wind tunnel). Inspection of the figure indicates that there is a region of wall–cylinder interaction which extends upward from the base to about 0.8 diameters above the base. Beyond that, the flow is unaffected by the presence of the wall, as witnessed by the uniformity of the pattern with height.

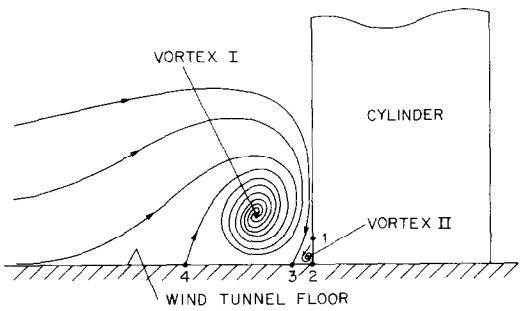

FIG. 5. Portrayal of the wall-adjacent flow pattern upstream of the stagnation line of the cylinder.

In the wall-unaffected region, there is a vertical stagnation line where the impinging flow strikes the cylinder head-on. The stagnation region is characterized by low velocities, so that the oil–lampblack mixture does not move. The flow splits at the stagnation line and streams circumferentially around each side of the cylinder, as indicated by the horizontal streaklines. At both edges of the photograph, there are black vertical strips with no streaks. The inboard edges of these strips mark the separation of the flow from the cylinder. Beyond this point, the cylinder-adjacent velocities are too low to produce streaks.

In the region of wall–cylinder interaction, the stagnation line gives way to a vertically downward flow which is also superposed on the circumferential flow which streams around the cylinder. To rationalize this downward flow, Fig. 5 has been prepared on the basis of

observations made during the present experiments and from information provided by the smoke photographs for a related flow field [5]. The figure portrays the wall-adjacent flow pattern upstream of the stagnation line of the cylinder. Shown there in a side view are two hypothesized vortices, whose respective cores are labeled I and II. The large Vortex I rotates clockwise and induces a downward flow whose effects were manifested in Fig. 3 by the disappearance of the vertical stagnation line and the downward angling of the streaks. Vortex II is much smaller than Vortex I and rotates counter-clockwise. From the visually observed rapid development of the oil–lampblack pattern in the neighborhood of Vortex II, it can be surmised that this vortex rotates much more rapidly than Vortex I.

Also shown in Fig. 5 are black dots numbered 1–4 depicting low velocity zones which can be identified in Figs. 3 and 4. In particular, Dot 1, situated directly above small Vortex II, appears in Fig. 3 as the prominent black band just above the base of the cylinder. Dot 2 corresponds to the very thin, hardly perceptible black band at the very base.

Figure 4 shows the flow pattern adjacent to the wind tunnel floor. The white circular area is the site of the cylinder, and the direction of the freestream flow is indicated by the arrows. Observation of the figure reveals a horseshoe-like pattern with its open end downstream. In actuality, there are two horseshoe-like structures which respectively correspond to Vortices I and II. To identify these and other features of the flow, it is convenient to imagine a traverse beginning at the forwardmost edge of the cylinder and moving upstream into the fluid.

The first feature encountered in such a traverse is a very thin black line immediately adjacent to the cylinder. This corresponds to the low-velocity pocket identified by Dot 2 in Fig. 5. The next feature is a white zone. Generally such a narrow white region indicates vigorous fluid motion. Here, it depicts the presence of Vortex II. Continued forward inspection reveals a somewhat wider black zone. This is a low velocity region situated between the two vortices as indicated by Dot 3 in Fig. 5. Beyond this black zone is a larger region populated with well-defined streaks. In the region forward of the cylinder, these streaks represent a backflow, as is consistent with the direction of rotation of Vortex I as shown in Fig. 5. The forward edge of this zone corresponds to the forward edge of the vortex, depicted by Dot 4.

These regions are swept around the sides of the cylinder, and their separate identities persist to the trailing edge of the cylinder, and beyond in the case of the large horseshoe vortex. It should be noted, however, that the inner black region enlarges and changes its nature beyond the separation point. At that point, it begins to enlarge and merges with the wake behind the cylinder (represented by the large black region downstream of the cylinder).

Certain aspects of the flow visualization will be revisited when the mass transfer results are presented.

Velocity profiles

Profiles of the streamwise velocity adjacent to the wind tunnel floor were measured to determine the extent of the boundary layer for the range of Reynolds numbers considered. As noted earlier, the measurements were made at the site of the cylinder but with the cylinder removed.

Figure 6 shows the results of these measurements. The ordinate is the velocity ratio u/u_∞, where u is the velocity at a given height y above the wind tunnel floor, and u_∞ is the freestream velocity. The abscissa is the dimensionless height y/d (d is the cylinder diameter). For reference purposes, the vertical dashed lines in Fig. 6 show the interfaces between the five positions of the sensing element. Profiles for three Reynolds numbers are plotted, respectively, 4000, 9700, and 23 000 and smooth curves have been faired through the data to provide continuity.

All three profiles are of similar shape. They rise steeply from the origin, then bend over and flatten out as the velocity ratio approaches unity. One of the

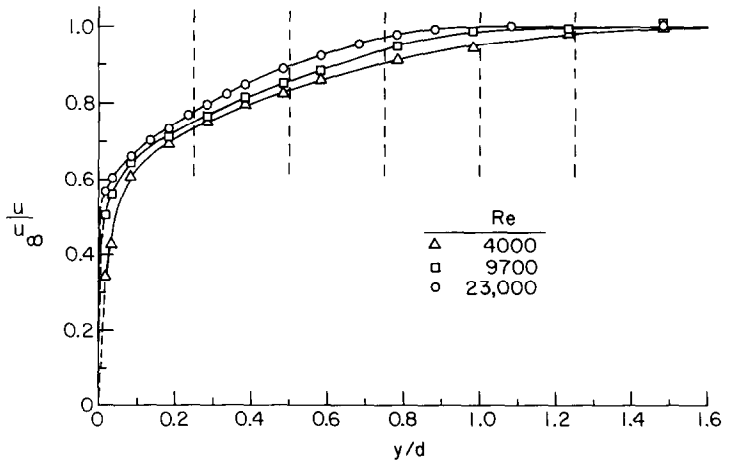

FIG. 6. Velocity profiles adjacent to the wind tunnel floor at the site of the cylinder.

significant differences between the profiles is the sharpness with which each profile bends over after it rises from the origin. The bending tends to be more gradual as the Reynolds number decreases. Correspondingly, the point where $u/u_\infty = 0.98$ varies from $y/d \simeq 0.8$ for the highest Reynolds number to $y/d \simeq 1.3$ for the lowest Reynolds number. These values of y/d can be regarded as the respective boundary layer thicknesses. It is worth noting that the aforementioned boundary layer thickness for the highest Reynolds number is approximately equal to the height of the wall-affected region identified from the flow visualization (i.e. Fig. 3).

It may also be noted that at $y/d = 1.25$, all of the profiles exceed $u/u_\infty = 0.975$. Therefore, $y/d = 1.25$ was the greatest height at which mass transfer measurements were made in the wall-adjacent region of the cylinder.

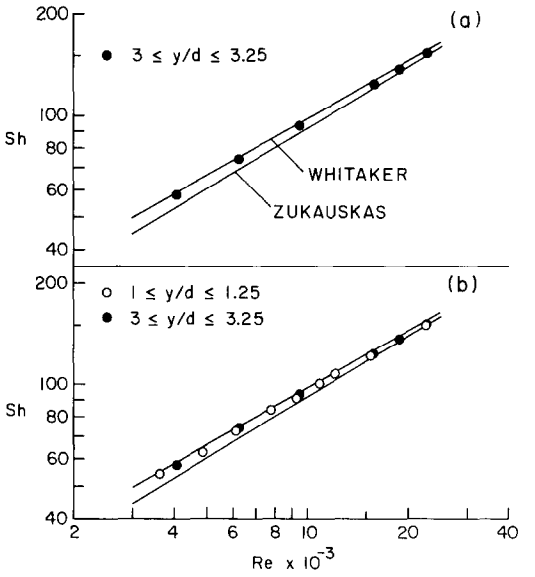

FIG. 7. Sherwood number results for the regions $3 \leqslant y/d \leqslant 3.25$ and $1 \leqslant y/d \leqslant 1.25$.

MASS TRANSFER RESULTS

Data reduction

As mentioned earlier, the amount of mass transferred from the surface of a sensing element was determined by measuring the mass of the element both before and after each data run. The mass flux $\dot{m}$ was then obtained by dividing the transferred mass by the naphthalene surface and by the duration of the run. From this, the mass transfer coefficient K and Sherwood number Sh were evaluated from their definitions

$$K = \dot{m}/(\rho_{nw} - \rho_{n\infty}),\ Sh = Kd/\mathscr{D}. \quad (1)$$

The naphthalene vapor density ρ_{nw} at the subliming surface was calculated from the Sogin vapor pressure relation and the perfect gas law, using the measured temperature of the sensing element as input. In the experiments, the freestream was pure air, so that $\rho_{n\infty} = 0$. The diffusion coefficient appearing in equation (1) was eliminated by employing the definition of the Schmidt number $Sc = \nu/\mathscr{D}$, in terms of which the Sherwood number can be written as $Sh = (Kd/\nu)Sc$ (with $Sc = 2.5$).

The impact−static pressure difference yielded the freestream velocity u_∞, from which the Reynolds number was evaluated in the standard manner

$$Re = u_\infty d/\nu. \quad (2)$$

Sherwood numbers

The first order of business is the presentation of the Sherwood number results for the wall-unaffected region and their comparison with heat transfer information from the literature. These data were collected with the sensing element positioned in the range $3 \leqslant y/d \leqslant 3.25$, and the corresponding Sherwood numbers are plotted as a function of the Reynolds number in Fig. 7(a). Also shown are two lines respectively representing the correlations of Zukauskas [2] and Whitaker [6] for heat transfer from a cylinder in crossflow. When these correlations are transformed from heat transfer to mass transfer terms by replacing the Nusselt and Prandtl numbers by the Sherwood and Schmidt numbers, there follows

$$Sh = 0.26Re^{0.6}\, Sc^{0.37},\ [2], \quad (3)$$

$$Sh = (0.4Re^{1/2} + 0.06Re^{2/3})Sc^{0.4},\ [6]. \quad (4)$$

The aforementioned correlations were selected from among others for the cylinder in crossflow because they are the only ones based on data for fluids of various Prandtl numbers (bracketing the Schmidt number of 2.5 of the present experiments). The other correlations are based on air data ($Pr = 0.7$), with a tacked-on factor of $Pr^{1/3}$. In general, from a review of all the available correlations, the extent to which they differ is remarkable. Furthermore, in all cases, there is considerable data scatter around the correlating line.

Turning now to Fig. 7, it is seen that the present data fall between the two correlating lines, tending to favor the Whitaker correlation at the lower Reynolds numbers. In light of the perspectives conveyed by the preceding paragraph, the agreement of the data with the literature can be regarded as very good. This level of agreement lends confidence to the naphthalene sublimation technique and its mode of application in the present experiments.

Attention is now turned to the Sherwood number results for the wall-adjacent region. These results are presented in separate graphs for each of the quarter diameter cylinder lengths at which the various sensing elements were positioned. The first of these graphs is for the region $1 \leqslant y/d \leqslant 1.25$, the second is for $0.75 \leqslant y/d \leqslant 1, \ldots$, and the last is for $0 \leqslant y/d \leqslant 0.25$.

Each graph has a common format. The Sherwood number data for the specific y/d range of interest are shown as open circles, while the black circles, taken from Fig. 7(a), correspond to the Sherwood numbers

for the wall-unaffected region. The two straight lines are those of Zukauskas and Whitaker. The black circles and the straight lines serve as reference information which will be used to identify the changes in the Sherwood number which occur as the wall–cylinder interface is more closely approached.

The results for the region $1 \leqslant y/d \leqslant 1.25$ are presented in Fig. 7(b), where they are seen to be virtually identical to those for the wall-unaffected region. The near-absence of wall effects at $1 \leqslant y/d \leqslant 1.25$ is not unexpected on the basis of the velocity profiles of Fig. 6 and the flow visualization pattern of Fig. 3.

Figures 8(a) and (b), respectively convey results for $0.75 \leqslant y/d \leqslant 1$ and for $0.5 \leqslant y/d \leqslant 0.75$. These graphs show a decrease of the Sherwood number as y/d decreases. On average, the decrease relative to the wall-unaffected results is 4% for $0.75 \leqslant y/d \leqslant 1$ and 10% for $0.5 \leqslant y/d \leqslant 0.75$. Overall, there is a tendency for stronger wall effects to occur at the lower Reynolds numbers.

A further decrease in the Sherwood number is sustained at $0.25 \leqslant y/d \leqslant 0.5$, as shown in Fig. 9(a). Here, on average, the Sherwood numbers are about 14% lower than those for the wall-unaffected region. Further decreases of the Sherwood number are, however, arrested and reversed at the lowermost sensing position, $0 \leqslant y/d \leqslant 0.25$, as can be seen by comparing Figs. 9(a) and (b). The comparison reveals a modest increase (about 5%) in the Sherwood numbers at the lowermost sensing position relative to those at the sensing position just above it, but they remain lower, by about 9%, than the Sherwood numbers for the wall-unaffected region.

The increased importance of wall–cylinder interactions with decreasing y/d is fully expected, both intuitively and on the basis of the fluid flow information conveyed by Figs. 3 and 6. However, it remains to

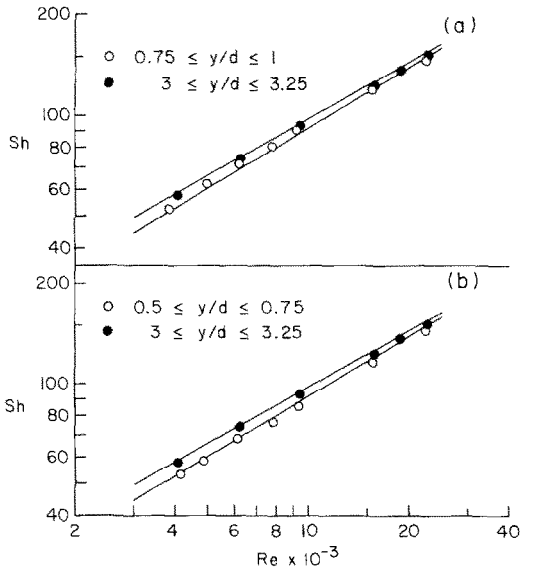

FIG. 8. Sherwood number results for the regions $0.75 \leqslant y/d \leqslant 1$ and $0.5 \leqslant y/d \leqslant 0.75$.

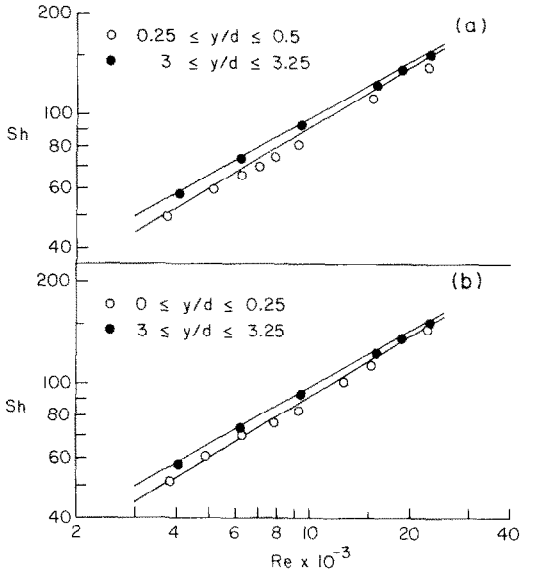

FIG. 9. Sherwood number results for the regions $0.25 \leqslant y/d \leqslant 0.5$ and $0 \leqslant y/d \leqslant 0.25$.

rationalize the trend toward decreasing Sherwood numbers with decreasing y/d in most of the wall-affected region and the reversal of this trend at the lowest sensing position.

To explain the decrease, it may be recalled that thicker boundary layers correspond to lower rates of transfer. In turn, the boundary layer thickness is increased for lower velocities and for longer lengths of flow path along the surface. In the wall-affected region, the velocities are lower than those at positions farther from the wall, as documented in Fig. 6. Further, considering the curved streak lines in evidence in the lower part of Fig. 3, it is evident that the path travelled by fluid particles in the wall-affected region is longer than that travelled by particles moving circumferentially around the cylinder. Thus, the decreased velocity and longer path length lead to diminished mass transfer in the wall-adjacent region.

With regard to the trend reversal at the lowest sensing position, it may be attributed to the presence of the small vortex (Vortex II of Fig. 5) that was discussed in connection with the flow visualization pattern. This vortex was observed to be very vigorous relative to the rest of the flow. Also, it is positioned at the base of the cylinder, immediately adjacent to the lowermost sensing position.

From the standpoint of practice, the extent of the Sherwood number reductions in the wall-adjacent region are of primary importance. These reductions have been identified in the description of Figs. 7–9 and will be given perspective in the concluding remarks.

CONCLUDING REMARKS

Quasi-local mass transfer measurements were made for a wall-attached cylinder in crossflow in order to determine how the transfer coefficients are affected by fluid flow interactions between the wall and the

cylinder. For the measurements, disk-like sensing elements were used which averaged over an axial length equal to a quarter of the cylinder diameter. The experiments spanned a Reynolds number range extending from about 3500 to 23 000. To supplement the mass transfer work, fluid flow experiments involving velocity profile measurements and flow visualization were also performed. The cylinder was sufficiently long so that the wall-adjacent region was not influenced by hydrodynamic and mass transfer happenings at the other end, which was free (i.e. unattached).

The mass transfer and velocity profile measurements and the flow visualization all indicated that the wall–cylinder interactions were confined to a length of cylinder extending about one diameter from the wall. The interactions caused a decrease in the transfer coefficients relative to those in the wall-unaffected region of the cylinder. These decreases were accentuated with decreasing distance from the wall, but this trend was reversed in the immediate neighborhood of the wall due to the presence of a compact, vigorous vortex.

The wall-related decreases in the cylinder transfer coefficients were moderate, with the largest quasi-local decrease being in the 15% range. For the entire affected region extending from the wall to a distance of one diameter from the wall, the decrease was about 9%. While these effects are not entirely negligible, they are not sufficiently large to invalidate present design procedures which ignore wall-induced decreases in the cylinder heat transfer coefficient.

With regard to wall–cylinder interactions in tube banks, the situation is made complicated by the cylinder-to-cylinder interactions. However, because of the latter, it is not unreasonable to expect that the wall boundary layers will be thinner than those for a single cylinder in crossflow. If this is so, then the wall-affected region should be less than the one diameter length encountered in the present experiments. If the overall length of a cylinder in the bank is substantially greater than one diameter, the wall–cylinder interactions should not have a major effect on the overall per-cylinder heat transfer.

Acknowledgement—The research reported here was performed under the auspices of the National Science Foundation.

REFERENCES

1. V. T. Morgan, The overall convective heat transfer from smooth circular cylinders, in *Advances in Heat Transfer*, Vol. 11, pp. 199–264. Academic Press, New York (1975).
2. A. A. Zukauskas, Heat transfer from tubes in crossflow, in *Advances in Heat Transfer*, Vol. 8, pp. 93–160. Academic Press, New York (1972).
3. J. Karni, The effects of a main stream boundary layer on heat transfer from a cylinder in crossflow, M.S. plan B project report, Department of Mechanical Engineering, University of Minnesota, Minneapolis, Minnesota (1982).
4. E. M. Sparrow and F. Samie, Measured heat transfer coefficients at and adjacent to the tip of a wall-attached cylinder in crossflow—applications to fins, *J. Heat Transfer* **103**, 778–784 (1981).
5. B. Thwaites, *Incompressible Aerodynamics*. Clarendon Press, Oxford (1960).
6. S. Whitaker, *Elementary Heat Transfer Analysis*. Pergamon Press, Oxford (1976).

TRANSFERT THERMIQUE ADJACENT A L'EXTREMITE ATTACHEE D'UN CYLINDRE EN ATTAQUE FRONTALE

Résumé—Des expériences en soufflerie sont conduites pour déterminer les coefficients de convection dans la région d'interaction paroi-cylindre pour un cylindre attaché à une paroi et attaqué frontalement. Des coefficients de convection quasi-locaux sont mesurés avec un petit élément sensible en forme de disque, positionné en différents endroits le long du cylindre. Les expériences couvrent un domaine de nombre de Reynolds entre 3500 et 23 000 et sont complétées par des mesures de profils de vitesse et une visualisation de l'écoulement. On trouve que les interactions paroi-cylindre sont confinées à une distance à la paroi d'environ un diamètre. Dans cette région d'interaction, les coefficients quasi-locaux sont inférieurs à ceux de la région non troublée. Les diminutions sont accentuées lorsque la distance à la paroi diminue, mais cette tendance est renversée au voisinage immédiat de la paroi à cause de la présence d'un tourbillon compact et vigoureux. La plus forte diminution est de 15% environ, tandis que la diminution moyenne pour toute la région d'interaction est de 9% environ.

WÄRMEÜBERGANG IM ENDBEREICH EINES AN EINER EBENEN WAND ANGEBRACHTEN QUER ANGESTRÖMTEN ZYLINDERS

Zusammenfassung Es wurden Versuche im Windkanal an einem quer angeströmten Zylinder, der an einer Wand angebracht war, zur Bestimmung des Wärmeübergangskoeffizienten im Gebiet der gegenseitigen Beeinflussung von Wand und Zylinder durchgeführt. Quasi-lokale Wärmeübergangskoeffizienten wurden mit einem kleinen scheibenförmigen Fühler (von der Länge eines viertel Durchmessers) gemessen. Dieses Meßelement wurde an verschiedenen Stellen entlang des Zylinders positioniert. Die Versuche wurden für Reynolds-Zahlen im Bereich von 3500 bis 23 000 durchgeführt und durch Messungen des Geschwindigkeitsprofils und Sichtbarmachung der Strömung ergänzt. Es wurde gefunden, daß die gegenseitige Beeinflussung zwischen Wand und Zylinder auf den Bereich eines Durchmessers von der Wand beschränkt ist. Die quasi-lokalen Wärmeübergangskoeffizienten sind im Wechselwirkungsbereich kleiner als die in dem von der Wand unbeeinflußten Gebiet. Die Abnahmen werden mit kleiner werdendem Wandabstand besonders spürbar. Diese Tendenz kehrt sich jedoch in unmittelbarer Wandnähe infolge eines kompakten kräftigen Wirbels um. Die größte Abnahme lag im Bereich um 15%, während die mittlere Abnahme für den gesamten von der Wand beeinflußten Bereich ungefähr 9% betrug.

ТЕПЛОПЕРЕНОС ВБЛИЗИ ПРИСОЕДИНЕННОЙ КОНЦЕВОЙ ЧАСТИ ПОПЕРЕЧНО ОБТЕКАЕМОГО ЦИЛИНДРА

Аннотация—Проведены эксперименты на аэродинамической трубе с целью определения коэффициентов теплопереноса для присоединенного к стенке поперечно обтекаемого цилиндра в области его взаимодействия со стенкой. Квазилокальные коэффициенты переноса измерялись с помощью небольшого (длиной в четверть диаметра) дискообразного элемента, помещаемого в разных местах по оси цилиндра. Эксперименты охватывали диапазон чисел Рейнольдса от 3500 до 23000. Кроме того, измерялись профили скорости и проводилась визуализация потока. Найдено, что взаимодействия между стенкой и цилиндром ограничиваются длиной цилиндра, выступающего на расстояние примерно одного диаметра от стенки. В области взаимодействия значения квазилокальных коэффициентов оказываются ниже значений в области, не подверженной влиянию стенки. Обращено внимание на то, что снижение значений происходило с уменьшением расстояния от стенки, но в непосредственной близости от нее возникала тенденция роста значений из-за влияния сильного компактного вихря. Самое большое снижение значений достигало 15%, а среднее — 9% для всей области, на которую распространялось влияние стенки.